Soft Matter

PAPER

View Article Online
View Journal | View Issue

Cite this: *Soft Matter*, 2017, **13**, 4252

Hybrid colloidal microswimmers through sequential capillary assembly†

Songbo Ni,[ab] Emanuele Marini,[ab] Ivo Buttinoni,[a] Heiko Wolf*[b] and Lucio Isa*[a]

Received 2nd March 2017,
Accepted 24th May 2017

DOI: 10.1039/c7sm00443e

rsc.li/soft-matter-journal

Active colloids, also known as artificial microswimmers, are self-propelled micro- and nanoparticles that convert uniform sources of fuel (*e.g.* chemical) or uniform external driving fields (*e.g.* magnetic or electric) into directed motion by virtue of asymmetry in their shape or composition. These materials are currently attracting enormous scientific attention as models for out-of-equilibrium systems and with the promise to be used as micro- and nanoscale devices. However, current fabrication of active colloids is limited in the choice of available materials, geometries, and modes of motion. Here, we use sequential capillarity-assisted particle assembly (sCAPA) to link microspheres of different materials into hybrid clusters of prescribed shapes (''colloidal molecules'') that can actively translate, circulate and rotate powered by asymmetric electro-hydrodynamic flows. We characterize the active motion of the clusters and highlight the range of parameters (composition and shape) that can be used to tune their trajectories. Further engineering provides active colloids that switch motion under external triggers or perform simple pick-up and transport tasks. By linking their design, realization and characterization, our findings enable and inspire both physicists and engineers to create customized active colloids to explore novel fundamental phenomena in active matter and to investigate materials and propulsion schemes that are compatible with future applications.

1. Introduction

Active colloids, or artificial microswimmers, are microscale objects that can convert available, uniformly distributed energy into directional propulsion due to an intrinsic asymmetry in either their composition or geometry. Directed motion can be generated autonomously from the environment or can be imparted by external fields. Autonomous active colloids self-propel by exploiting surrounding chemical ''fuels'',[1–4] while externally activated colloids rather swim due to a local force induced by different sources, such as magnetic,[5,6] electric,[7] optical,[8,9] and ultrasonic fields.[10,11] As such, active colloids are a paradigmatic example of internally driven out-of-equilibrium thermodynamic systems, for which a broad range of emergent phenomena has been discovered, including chaining,[12] clustering,[13,14] swarming,[15] and phase separations.[16] Moreover, they are central for the pursuit of miniaturized micro- and nanomachines, a vision that is beginning to take form with first proof-of-principle examples of autonomously powered micro-gears[17–19] and of vehicles for drug delivery[20–22] or other cargoes,[23] in environmental remediation,[24,25] and for lab-on-chip immunoassays.[26]

While many strategies have been developed to date to fabricate active colloids,[3,27,28] the vast majority of these efforts is restricted to the study of particles with simple shapes and compositions. Synthetic active colloids in fact most often consist of individual patchy spheres[2] or rods.[1] However, recent experiments and numerical simulations demonstrated that the simultaneous presence of propulsive forces and internal torques, due to the shape-anisotropy or bottom-heaviness of the particles,[29] greatly enriches the properties of the resulting active trajectories. Active chiral particles can for instance circulate,[30] respond to gravitational fields[31] or be guided in microfluidic devices.[32,33] These results represent the first attempts towards the realization of active colloids with modes of motion that are prescribed by their symmetry. These ideas have then been taken further by numerical simulations of active clusters prepared by computing the controlled assembly of single active beads into tailored objects (*e.g.*, clusters assembled using combinations of ''pushers'' and ''pullers'',[34,35] or beads with different surface electric properties[36,37]). Doing so experimentally is more challenging and commonly recognized as one of the major hurdles preventing the further development of active colloids in a broad range of applications.[38,39] A method that allows the

[a] *Laboratory for Interfaces, Soft Matter, and Assembly, Department of Materials, ETH Zurich, Vladimir-Prelog-Weg 5, 8093 Zurich, Switzerland. E-mail: lucio.isa@mat.ethz.ch*

[b] *IBM Research – Zurich, Säumerstrasse 4, 8803 Rüschlikon, Switzerland. E-mail: hwo@zurich.ibm.com*

† Electronic supplementary information (ESI) available. See DOI: 10.1039/c7sm00443e

fabrication of synthetic microswimmers with full programmability in the choice of materials, composition and shape remains elusive.

Here, we use sequential capillarity-assisted particle assembly (sCAPA) to demonstrate the realization of a library of multi-material, or hybrid, active "colloidal molecules" (CMs), *i.e.* clusters of microspheres assembled in prescribed geometries,[40] whose swimming velocity and type of motion can be rationally designed by independently choosing their composition and shape. sCAPA is a recently developed method[40,41] that enables the full programmability of hybrid colloidal molecules, here applied to the realization of versatile microswimmers.

Actuation of asymmetric CMs can be realized in different ways.[1–11] Here, we use electro-hydrodynamic flows to power active CMs moving over an electrode in a vertical AC electric field. The actuation mechanism was recently described using a simple colloidal molecule,[7] *i.e.* an asymmetric dimer. A dielectric particle near an electrode deforms the vertical electric field, which develops tangential components able to locally drive induced charges on the electrode and trigger electro-hydrodynamic (EHD) flows.[42] The EHD flow is highly dependent on surface chemistry, dielectric properties, surface charge and geometry of the colloidal particles, and is symmetric around spherical or homogeneous particles. However, introducing compositional or geometrical variations, *e.g.* in a heterogeneous dimer, breaks the symmetry and unbalanced EHD flows drive net propulsion. The direction and speed of this active motion are determined by the geometry and the degree of asymmetry generated by the properties of the individual components of the specific colloidal molecule. Even though direct experimental access to all these quantities remains elusive, theoretical and experimental[7,42] studies show that the speed of the EHD flows, and thus the swimming speed of the active CMs, is proportional to the field strength squared, affording facile control of the propulsion velocity with an external control parameter.

In this work, we exploit the same driving mechanism to induce the self-propulsion of customized active colloidal molecules produced by sCAPA. We demonstrate the link between design, realization and characterization of the motion of hybrid colloidal microswimmers made out of different materials and with geometries that make them translate at various speeds, circulate and rotate. We also demonstrate more complex objects, which can switch between these modes of motion and even perform simple cargo pick-up and transport tasks. The various classes of active colloids are presented, followed by a detailed description of the experimental methodology. This paper closes with a critical discussion of our findings suggesting possible directions for future developments.

2. Results

The fabrication, harvesting and actuation process of the CMs is shown in Fig. 1a and more details are given in the

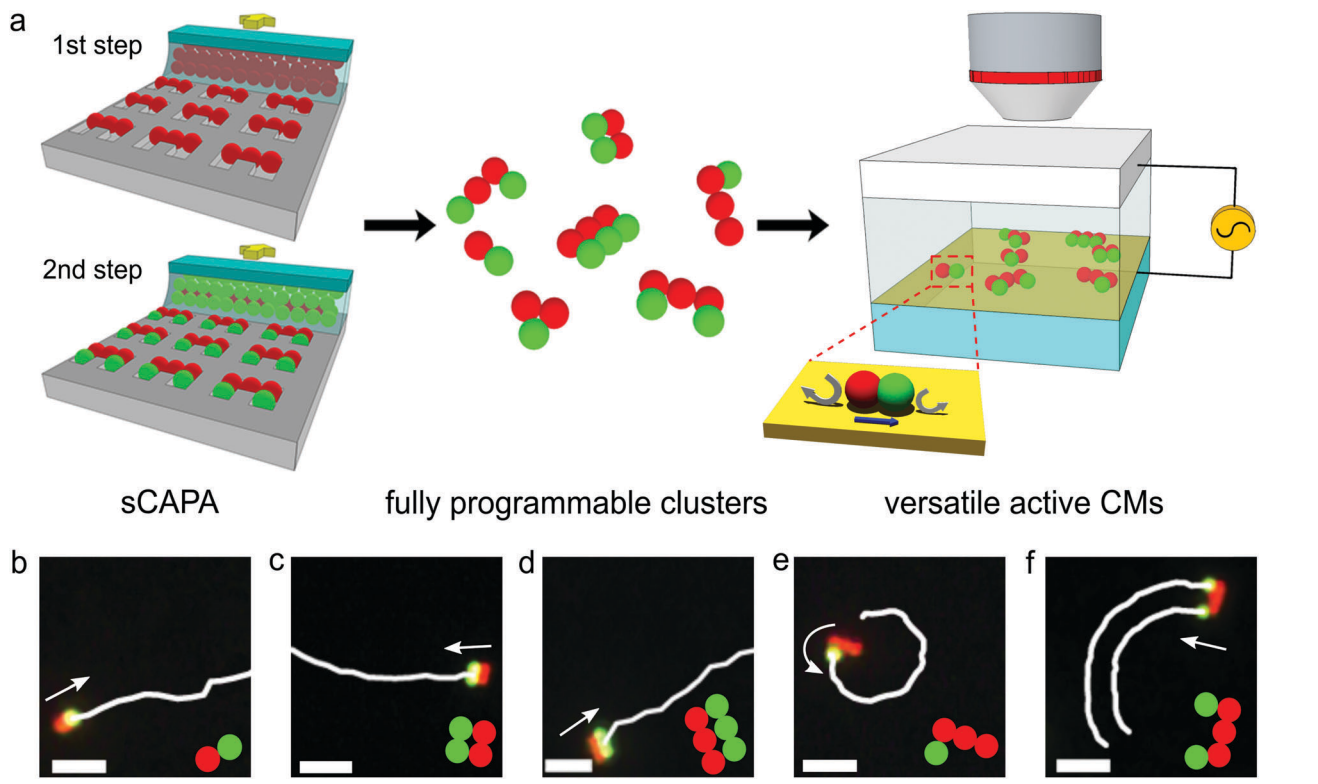

Fig. 1 Fabrication of active colloidal molecules. (a) Scheme of the process from the assembly of CMs by sCAPA, to the harvesting and actuation in an AC electric field. The zoom schematically illustrates a possible unbalanced EHD flow around a dumbbell-like CM. (b–f) Fluorescence microscopy snapshots overlaid with the trajectories of colloidal miscroswimmers of different geometries. The insets schematically show the details of the structures of the CMs. The arrows represent the directions of motion. The scale bars are 5 μm.

Experimental section. Briefly, microspheres from different materials are sequentially assembled in templates using sCAPA.[40] The geometry of the template defines the shape of the CMs, and the assembly sequence determines their composition. The assembly of all CMs is detailed in Fig. S1 (ESI†). After assembly and linking *via* sintering, CMs are harvested and dispersed in water. They are subsequently confined in an observation cell that consists of a bottom gold electrode, a top ITO electrode and a PDMS spacer with a thickness between 200 μm and 300 μm. AC electric fields with peak-to-peak voltages V_{pp} between 4 and 30 V and frequencies from 500 Hz to 1.5 kHz are applied to actuate the CMs. The zoom in Fig. 1a shows a sketch of the unbalanced EHD flows around a dumbbell-like CM. In this work, we fabricate and characterize a library of complex active CMs with shapes beyond dumbbells and with multiple material combinations. Examples of isolated CMs that translate and rotate are given in Fig. 1b–f and Movie S1–S5 (ESI†). They are constructed using amine-functionalized (green, 1.1 μm) and non-functionalized (red, 1 μm) polystyrene (PS) particles (see the Experimental section for more details).

One of the main advantages of sCAPA is its flexibility in integrating different materials into a single CM, allowing a broad spectrum of combinations of functional properties. To demonstrate the impact that material choice has on the motion of active CMs, we have fabricated dumbbell-like microswimmers combining both organic PS particles (non-functionalized and amine-functionalized) and inorganic particles of SiO_2, TiO_2 and SiO_2 with embedded magnetic nanoparticles (henceforth referred to as SiO_2-Mag). Additional details are given in the ESI,† Fig. S2. All of them exhibit self-propulsion, and their swimming speed v and rotational diffusion time τ_R are calculated from the particle trajectories, respectively extracting the speed by fitting their short-time-scale mean square displacements and obtaining τ_R as a characteristic time scale for the decorrelation of the direction of their velocity vectors (see the Experimental section).

For all these dumbbells, v increases linearly with the square of the field strength (Fig. S3, ESI†), which is characteristic of propulsion from EHD flows.[7,42] We furthermore demonstrate that the swimming speed can be tuned by choosing different material combinations, while leaving the external field and the rotational diffusion time unaltered (Fig. 2a inset). Fig. 2a shows the swimming speed of different dumbbell-like CMs, with the schemes indicating the propulsion direction. The variation in the swimming speed between the different types of dumbbells is attributed to the variations in the dielectric properties of the particles composing the lobes, *i.e.* their zeta potential ζ and Stern layer conductance σ. Quantitative predictive power of the swimming velocity, and even on its direction, remains however an open issue. Examining the values of the zeta potential alone for each of the dumbbell lobes (see Fig. S8 in the ESI†) for instance cannot fully explain the ranking and the values of the measured swimming velocity. In particular, in the measurement's conditions, SiO_2 and PS particles have practically a negligible difference in ζ and yet the PS/SiO_2 dumbbells move with a significant speed. Similarly, dumbbells with PS–NH_2/SiO_2 move with the silica lobe at the back (Fig. 2a), while PS/TiO_2 dumbbells move with the PS lobe at the back, in spite of the fact that

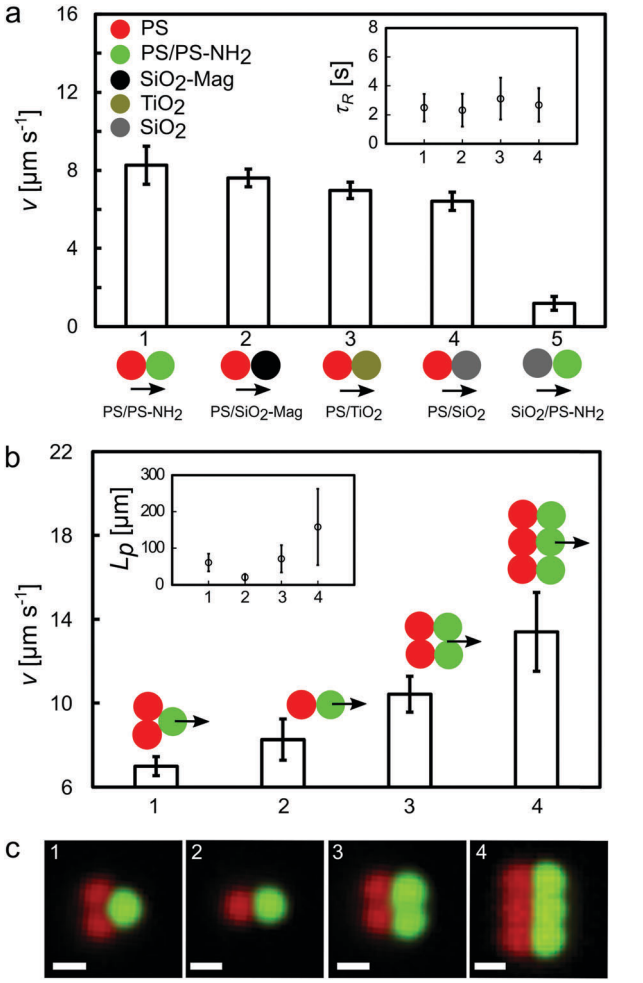

Fig. 2 Translating active colloidal molecules in different materials and shapes. (a) Swimming velocities v plotted for dumbbell-like active CMs in different material combinations, with an applied field of 32 V mm^{-1} at 1.3 kHz. Different materials are labeled in different colors as indicated in the legend. The schemes below the horizontal axis depict the corresponding dumbbells and their propulsion directions. The inset shows the rotational diffusion time τ_R for the microswimmers in the same order. Note that for the PS–NH_2/SiO_2 combination, due to the low value of the propulsion speed, accurate determination of τ_R with the velocity autocorrelation method is not possible because of thermal fluctuations; therefore, the corresponding data point is not shown in the inset. (b) Ranking of v for active CMs of different shapes, with an applied field of 32 V mm^{-1} at 1.3 kHz. The arrows show the propulsion directions. The inset reports the persistence length L_p of the active CMs. The fluorescence images in (c) show the corresponding active CMs labeled by the same numbers. The scale bars are 1 μm.

$|\zeta_{TiO_2}| > |\zeta_{PS}|$ and $|\zeta_{SiO_2}| > |\zeta_{PS\text{–}NH_2}|$. These uncertainties are connected to the challenging determination of the Stern layer conductance, which is sensitive to the details of surface composition and its charging mechanism, and the distance between each lobe of the dumbbell and the bottom electrode.[7] Further experimental work is needed in this direction and numerical simulations solving the full electro-hydrodynamic flows around particles of complex shapes will be essential to gain predictive power. Even in the absence of quantitative predictions, the versatility of sCAPA in material choice enables the incorporation of functional particles in the active CMs, *e.g.*, catalytic TiO_2 and magnetic SiO_2-Mag moieties,

opening future avenues for the fabrication of new types of artificial microswimmers.

Full control on the colloidal molecules' shape is another key advantage of sCAPA. Using more complex assembly templates, we demonstrate that simple variations in the CMs' geometry tremendously affect their ability to follow long straight paths, *i.e.*, influence the persistency of their active trajectories. Fig. 2b shows a range of different translating microswimmers (see Fig. S2 and S4 for details of their structure, ESI†) whose trajectories' persistence lengths $L_p = v \cdot \tau_R$ span more than two orders of magnitude. In contrast, v and L_p are decoupled by changing the architecture, so that a trimer and a "four-pack" have similar persistence lengths, but different propulsion velocities (CM type 1 and 3 in Fig. 2b and c). Analogously, dumbbells and "six-pack" rectangular clusters have swimming velocities that differ only by a factor 2, but display very different persistency (CM type 2 and 4 in Fig. 2b and c). Although the same above-mentioned remarks apply here to the exact link between particle shape and propulsion speed, our findings indicate that specific trajectories of our active CMs can be successfully engineered. We can design, for instance, CMs that move in straight lines over large distances for effective transport in long narrow channels or CMs that reorient frequently to promote effective local remediation or motion in tortuous porous media. The independent control of composition and geometry affords the independent tuning of swimming velocity and persistency.

The ability to control the shape and composition of our active CMs enables rational design not only for tuning translational motion but also for enabling more complex modes of motion. This is demonstrated by fabricating and characterizing colloidal rotors and L-shaped swimmers that can switch their mode of motion from circular to translational upon application of high-frequency electric pulses.

Fig. 3a and its insets show a fluorescence image, an SEM image and the assembly scheme of colloidal rotors. The assembly is done in a trap that is slightly wider than the particle diameter (1.6 μm *versus* 1–1.1 μm), and sequential filling results in two active dumbbell units forming a zig-zag CM (see Fig. S1 for details, ESI†). Propulsion of the two dumbbell units in opposite directions, but with an offset, generates a torque and causes the CM to rotate on the spot[43] (inset to Fig. 3b). The CM's angular speed depends linearly on the square of the field strength (Fig. 3b), analogous to the propulsion of dumbbells, implying facile external control in applications. Fig. 3c shows snapshots of the rotation at different times (Movie S6, ESI†). Fig. 3d shows instead a fluorescence image, an SEM image, and the assembly scheme of L-shaped CMs (see Fig. S1 for assembly details, ESI†). Because of the propulsion along the short arms (*i.e.*, by a dumbbell), a torque is established along with directed propulsion,[30] and the activated CM moves circularly as shown in Fig. 3e and 1e. The engineering of L-shaped CMs can be extended so that switching between different modes of motion becomes possible. We have fabricated a second type of L-shaped CMs containing another green PS–NH_2 particle at the end of the long arm (see Fig. S1 for assembly details, ESI†), as shown in Fig. 3f and its inset, leading to propulsion along both arms. Their successful

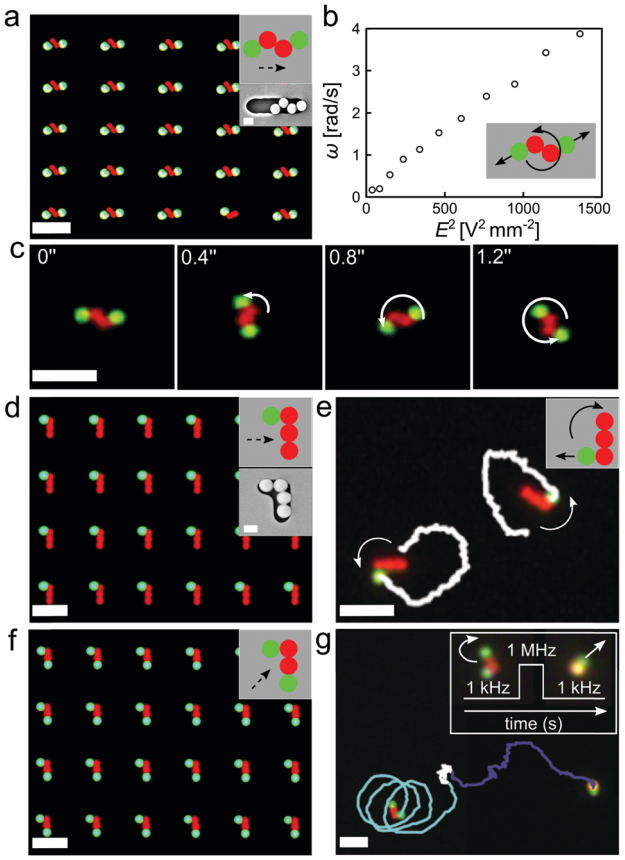

Fig. 3 Anisotropic microswimmers with versatile modes of motion: rotational, circular and reconfigurable motion. (a–c) Rotating microswimmers. (a) Fluorescence image of colloidal rotors on the template. The insets show the scheme of the structure of the CMs (the dashed arrow represents the assembly direction) and an SEM image of a colloidal rotor on the template. (b) Rotation speed ω plotted *versus* the square of the electric field, E^2. ω increases linearly with E^2 as the speed v does for the translating CMs. The inset schematically illustrates the rotation mechanism. (c) Snapshots of the CM in rotation at different times. (d and e) Circulating microswimmers. (d) Fluorescence image of L-shaped CMs on the template. The insets also show the corresponding scheme of the structure's assembly and an SEM image of the CM on the template. (e) Snapshot of L-shaped microswimmers during circular motion, overlaid with their trajectories. The solid arrows represent the directions of circular motion, whose mechanism is illustrated in the inset. (f and g) Reconfigurable CMs. (f) Fluorescence image of L-shaped active CMs with propulsion along two arms on the template. The inset again shows the CM scheme and the assembly direction (dashed arrow). (g) Trajectory showing the switch from circular (blue) to translational (purple) motion, overlaid with the initial and the last frame. The inset depicts the sequence of applied field frequency (E = 28 V mm^{-1}) and the corresponding switch in microswimmer orientation. The scale bars are 5 μm in (a–g) and 1 μm in the insets of (a and d).

fabrication relies on the precise control of the assembly direction with respect to the geometry of the L-shaped traps (see Fig. S1 for more details, ESI†). In Fig. 3g and Movie S7 (ESI†), we demonstrate that the second type of L-shaped CMs switches from circular to translational motion upon changing the frequency of the driving field to modify the CM's orientation relative to the substrate (see the inset in Fig. 3g). Initially the CM lies flat on the substrate and exhibits circular motion at 1 kHz. Increasing the AC frequency to 1 MHz causes the CM to stop its propelling

motion and to stand upright, aligning the long arm with the electric field, as previously observed for other anisotropic particles.[44] When the frequency is switched back to 1 kHz, the CM has no time to reorient, and translates with the short arm on the substrate. The possibility of propulsion along both arms ensures that the switch from circular to translational motion takes also place if the short arm aligns with the MHz field (see Movie S8, ESI†), as opposed to the first type of L-shaped CMs. The reverse switch from translational back to circular motion is achieved by turning off the field, waiting for the CMs to lie flat again and finally turning the field on at 1 kHz. This simple example demonstrates the capability of appropriately designed multi-functional colloidal clusters to act as reconfigurable smart motors.

Finally, simple specific tasks can be performed by rationally engineering anisotropic colloidal microswimmers. As a proof of concept, here, a specifically tailored CM is designed to "pick up", guide, transport, and release micro-objects. We performed "pick-up" tests for different CM shapes in a controlled environment defined by gold electrodes patterned by stripes (Fig. 4a). The stripe generates an electro-hydrodynamic flow[45,46] that confines the CM within the pattern, but allows it to move along it (Fig. 4b and Movie S9, ESI†). This serves the purpose to confine the targets and the active CM to increase "pick-up" rates and display the rationale behind their design. Fig. 4b and Movie S9 (ESI†) show a dumbbell-like CM that travels in a straight line on the patterned electrode for a distance ($\approx$80 μm in Movie S9, ESI†) much larger than its persistence length ($\approx$20 μm).

We discuss three different designs of CMs that are potentially able to pick up and transfer a micro-object: a "four-pack" (two dumbbells in parallel, Fig. S4, ESI†), a "six-pack" (three dumbbells in parallel, Fig. S4, ESI†) and a U-shaped CM. Single PS and PS–NH_2 spheres are intentionally dispersed to serve as cargoes.

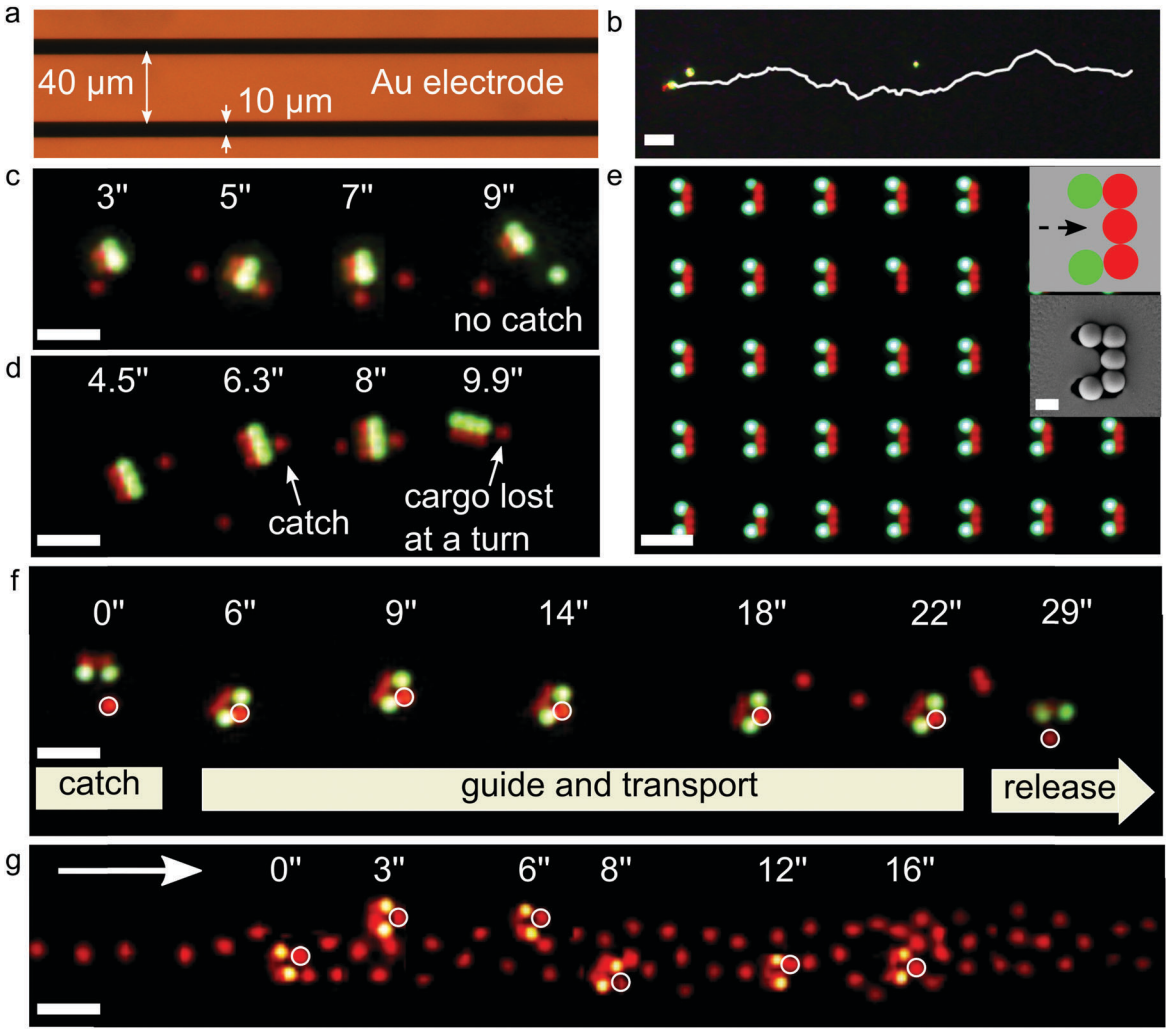

Fig. 4 Colloidal transporters: guiding, design and performance. (a) Patterned electrode to guide active CMs. (b) Dumbbell-like microswimmer traveling straight along the electrode. (c and d) Performance of "four-pack" (c) and "six-pack" (d) colloidal transporters illustrated by a time series of fluorescence images. (e) Assembly of U-shaped CMs, with their scheme and SEM image in the inset. The dashed arrow represents the assembly direction. (f and g) U-shaped active CMs transport a cargo particle in an empty and in a crowded environment. The solid arrows represent the guiding and transport directions. Note that the actual distance traveled is larger than the image size because of the movement of the stage to follow the active CMs (see Movie S12 and S14, ESI†). Scale bars are 5 μm (b–g) and 1 μm in the inset of (e).

Movie S10 (ESI†) and Fig. 4c show the "four-pack" CM in action. The small cross section perpendicular to the moving direction leads to failure to pick up any particles. An improvement is seen by increasing the cross section using a "six-pack". Movie S11 (ESI†) and Fig. 4d reveal that a "six-pack" CM can pick up a target particle, but that it loses it when changing direction. To protect the cargo during transport and avoid its loss during changes of direction, we designed and fabricated U-shaped microswimmers as shown in Fig. 4e (for assembly details, see Fig. S1, ESI†). Fig. 4f shows a time series demonstrating that these U-shaped CMs effectively pick up and transport a cargo along the patterned electrode stripe when the field is on and release it when the field is turned off (Movie S12, ESI†). The effectiveness of this design is also demonstrated by showing that different types of target particles can be captured (PS–NH_2, Fig. S6 and Movie S13, ESI†) and transported, even in crowded environments (Fig. 4g and Movie S14, ESI†). The only failure mode observed in crowded environments is the exchange of the particle being transported with another one, as shown in Fig. S7 and Movie S15 (ESI†). This proof of concept shows how the design of CMs can be used to define and optimize their function, and forms the basis for future implementations in which the geometry (longer side arms) or the material composition (magnetic beads for remote steering) can be tailored for specific applications.

3. Experimental

Colloidal suspensions

Fluorescent non-functionalized PS particles with a diameter of 1 μm (red, R0100, polydispersity <5%) and plain silica particles with a diameter of 1 μm (8100; polydispersity <5%) were purchased from Thermo Scientific. Fluorescent amine-functionalized PS particles with a diameter of 1.1 μm (green, F-8765, polydispersity <5%) were purchased from Life Technologies. Magnetic particles (iron-oxide nanoparticles in a silica matrix) with a diameter of 0.96 ± 0.05 μm (SiO_2-MAG-AR359) were purchased from micro-Particles GmbH. Titania (TiO_2) particles with a diameter of 1 μm (C-TIO-1.0, polydispersity <5%) were purchased from Corpuscolar Inc. The zeta potential for all particles was measured by a Zetasizer Nano (Malvern) and can be found in Fig. S8 (ESI†).

Fabrication of active colloidal molecules

The fabrication of the assembly template in PDMS (poly(dimethylsiloxane)), the sequential capillarity-assisted particle assembly, the linking, printing and harvesting of the CMs are all done according to the protocol reported in ref. 40.

Actuation by a vertical AC field

Aqueous suspensions of CMs fabricated by sequential capillarity-assisted particle assembly were placed in a cell consisting of a bottom gold electrode (100 nm of gold evaporated on a glass slide), a top ITO electrode and a PDMS spacer with a thickness between 200 μm and 300 μm. The colloids were actuated by AC fields with peak-to-peak voltages V_{pp} between 4 and 30 V and frequencies from 500 Hz to 1.5 kHz (AC function generator, Agilent 33250A).

Switching of the motion modality of L-shape microswimmers was performed with an applied AC electric field of 20 V_{pp} and a spacer of 230 μm. The motion of the CMs was switched and controlled by changing the frequency from 1 kHz to 1 MHz and back to 1 kHz.

Guiding of CMs was performed on patterned gold electrodes. The electrodes were prepared by optical lithography and metal deposition (e-beam physical-vapor deposition, 100 nm Au) followed by a lift-off step.

Imaging and analysis

CMs assembled on the template or printed on a substrate were imaged by bright-field, dark-field, and fluorescence optical microscopy (single-filter or dual-filter, Zeiss Axioscope) at various magnifications and by SEM (Leo 1550 Gemini, Carl Zeiss AG). ImageJ (W. S. Rasband, National Institutes of Health, Bethesda, MD) was used to compose overlays of fluorescence and bright-field images by combining different channels. All movies were grabbed at a frame rate of 7 or 10 fps using a dual filter in fluorescence optical microscopy, or using bright-field microscopy and a CCD camera. For aesthetic reasons, frames in Fig. 3g, 4b–d, f–g and Fig. S6, S7 (ESI†) were rotated by 90° as compared to the original movies.

The positions of the colloidal microswimmers were acquired by tracking one particle using either an ImageJ plugin, customized software written in Matlab (MathWorks) or IDL (Harris Geospatial). The coordinates of the tracked particle in each frame were used to calculate the swimming speed according to ref. 47. The mean square displacement (msd) $\langle[\Delta L(t)]^2\rangle$ was plotted against time t, which can be expressed by the following equation:[48]

$$\left\langle[\Delta L(t)]^2\right\rangle = \left(4D_0 + 2v^2\tau_R\right)t + 2v^2{\tau_R}^2\left(e^{-\frac{t}{\tau_R}} - 1\right), \quad (1)$$

and for times close to the rotational diffusion time τ_R, the msd curve can be fitted by the following equation after a second-order expansion:

$$\langle[\Delta L(t)]^2\rangle = 4D_0t + v^2t^2, \quad (2)$$

where D_0 is the 2D translational diffusion coefficient of a passive CM and v is its swimming speed. D_0 can be measured from the slope of the MSD of the passive CMs without any external field applied. The translational diffusion coefficients of a passive dumbbell, a passive triangle, a passive "four-pack" and a passive "six-pack" cluster were measured to be 0.179 $\mu m^2\ s^{-1}$, 0.148 $\mu m^2\ s^{-1}$, 0.097 $\mu m^2\ s^{-1}$, and 0.058 $\mu m^2\ s^{-1}$, respectively.

The rotational diffusion time τ_R was estimated according to ref. 49 and 50, based on the analysis of the time correlation between the directions of the swimming speeds from an initial time t_0 and after a time lag t, $V(t_0)$, and $V(t)$, respectively. As the swimming steps are much larger than the Brownian fluctuations, τ_R can be extracted using the following fitting for the correlation curve:

$$\langle \underline{V}(t)\cdot\underline{V}(t_0)\rangle = v^2e^{-t/\tau_R} \quad (3)$$

4. Discussion and conclusions

Our results demonstrate that sCAPA enables an unprecedented level of engineering of a variety of colloidal molecules that

actively move in spatially uniform vertical AC electric fields. The CMs are prepared from different materials and in various shapes. They can be tailored and designed to translate, rotate, switch the type of motion, and even pick up and transport cargoes. Given the flexibility that sCAPA provides in rationally designing and fabricating multifunctional clusters of colloidal particles, one can easily envision the fabrication of CMs powered by mechanisms other than electro-hydrodynamic flows or even by a combination of mechanisms. Future developments include scaling-up of particle production, downsizing of the assembled CMs towards the nanoscale and the development of predictive power to link the geometry, composition and propulsion strategies of the CMs to their active behaviour, accompanying experiments with numerical simulations. The challenges of scaling up fabrication increase as the structure of colloidal molecules becomes more complex. While the current throughput of dimers can reach a few millions per hour with a nearly 100% uniformity, more complex colloidal molecules require future process optimization (*e.g.* higher fidelity of the template and engineering of the meniscus shape) to increase the uniformity and thus the throughput. The size of the assembled particles can be reduced[51] and currently sCAPA of nanoparticles is being performed to test the limits of the method. Finally, increasing the complexity of CMs in the future also calls for in-depth fundamental studies to develop predictive power in the design of specific CMs with tailored motion and function.

Colloidal particles or clusters exhibiting directional and specific interactions with prescribed symmetries have also attracted enormous interest as building blocks for complex 3D materials' assembly. Notable examples include objects with shapes (and interaction potentials) that resemble the ones of simple molecules,[52,53] and even display internal degrees of freedom that lead to different "isotopes" of the same species,[54] mimicking natural structures at atomic scales. Very recently, DNA-coated particles introducing specific interaction symmetries have even been used to assemble large-scale crystalline structures with no atomic analogues.[55] Even though it would be tempting to consider sCAPA an additional route to produce asymmetric colloidal building blocks, the throughput of our fabrication methodology in terms of particle numbers[40] makes this option practically not viable for 3D assembly of macroscopic materials. The strength and uniqueness of the method instead lie in the opportunity to realize microscale objects that cannot otherwise be made, and where the individual hybrid colloid itself can start to be considered as a small device. This extended design flexibility may constitute a next step toward the realization of colloidal micro- and nanomachines, where their fabrication and the characterization of their active motion can be closely linked.

In conclusion, we envision sCAPA to become a powerful toolbox for the parallel fabrication of customized active colloids. Engineering of particle geometry and composition will help identify new propulsion schemes, screen and test the compatibility of the active colloids towards practical micro- and nanodevices and may contribute to unravel the complexity of the active systems ubiquitously found in nature.

Acknowledgements

We thank U. Drechsler, R. Stutz and S. Reidt for help with the mask and master fabrication, A. Knoll, U. Duerig, K. Carroll, H. Löwen and B. ten Hagen for discussions and advice, C. Bolliger for assistance with the manuscript, and R. Allenspach and W. Riess for continuous support. L. I., S. N., and I. B. acknowledge financial support from the Swiss National Science Foundation (grant PP00P2_144646/1).

References

1 W. F. Paxton, K. C. Kistler, C. C. Olmeda, A. Sen, S. K. St. Angelo, Y. Cao, T. E. Mallouk, P. E. Lammert and V. H. Crespi, *J. Am. Chem. Soc.*, 2004, **126**, 13424–13431.
2 J. Howse, R. Jones, A. Ryan, T. Gough, R. Vafabakhsh and R. Golestanian, *Phys. Rev. Lett.*, 2007, **99**, 048102.
3 S. Sánchez, L. Soler and J. Katuri, *Angew. Chem., Int. Ed.*, 2015, **54**, 1414–1444.
4 W. Wang, W. Duan, S. Ahmed, T. E. Mallouk and A. Sen, *Nano Today*, 2013, **8**, 531–554.
5 R. Dreyfus, J. Baudry, M. L. Roper, M. Fermigier, H. A. Stone and J. Bibette, *Nature*, 2005, **437**, 862–865.
6 L. Zhang, J. J. Abbott, L. Dong, K. E. Peyer, B. E. Kratochvil, H. Zhang, C. Bergeles and B. J. Nelson, *Nano Lett.*, 2009, **9**, 3663–3667.
7 F. Ma, X. Yang, H. Zhao and N. Wu, *Phys. Rev. Lett.*, 2015, **115**, 208302.
8 I. Buttinoni, G. Volpe, F. Kümmel, G. Volpe and C. Bechinger, *J. Phys.: Condens. Matter*, 2012, **24**, 284129.
9 A. P. Bregulla, H. Yang and F. Cichos, *ACS Nano*, 2014, **8**, 6542–6550.
10 W. Wang, L. A. Castro, M. Hoyos and T. E. Mallouk, *ACS Nano*, 2012, **6**, 6122–6132.
11 D. Kagan, M. J. Benchimol, J. C. Claussen, E. Chuluun-Erdene, S. Esener and J. Wang, *Angew. Chem., Int. Ed.*, 2012, **51**, 7519–7522.
12 J. Yan, M. Han, J. Zhang, C. Xu, E. Luijten and S. Granick, *Nat. Mater.*, 2016, **15**, 1095–1099.
13 J. Palacci, S. Sacanna, A. P. Steinberg, D. J. Pine and P. M. Chaikin, *Science*, 2013, **339**, 936–940.
14 J. Zhang, J. Yan and S. Granick, *Angew. Chem., Int. Ed.*, 2016, **55**, 5166–5169.
15 A. Bricard, J.-B. Caussin, N. Desreumaux, O. Dauchot and D. Bartolo, *Nature*, 2013, **503**, 95–98.
16 I. Buttinoni, J. Bialké, F. Kümmel, H. Löwen, C. Bechinger and T. Speck, *Phys. Rev. Lett.*, 2013, **110**, 238301.
17 R. Di Leonardo, L. Angelani, D. Dell'Arciprete, G. Ruocco, V. Iebba, S. Schippa, M. P. Conte, F. Mecarini, F. De Angelis and E. Di Fabrizio, *Proc. Natl. Acad. Sci. U. S. A.*, 2010, **107**, 9541–9545.
18 A. Sokolov, M. M. Apodaca, B. A. Grzybowski and I. S. Aranson, *Proc. Natl. Acad. Sci. U. S. A.*, 2010, **107**, 969–974.
19 C. Maggi, J. Simmchen, F. Saglimbeni, J. Katuri, M. Dipalo, F. De Angelis, S. Sanchez and R. Di Leonardo, *Small*, 2016, **12**, 446–451.

20 G. Dogangil, O. Ergeneman, J. J. Abbott, S. Pane, H. Hall, S. Muntwyler and B. J. Nelson, *Toward targeted retinal drug delivery with wireless magnetic microrobots*, 2008.
21 W. Gao, R. Dong, S. Thamphiwatana, J. Li, W. Gao, L. Zhang and J. Wang, *ACS Nano*, 2015, **9**, 117–123.
22 S. Sundararajan, P. E. Lammert, A. W. Zudans, V. H. Crespi and A. Sen, *Nano Lett.*, 2008, **8**, 1271–1276.
23 L. Baraban, M. Tasinkevych, M. N. Popescu, S. Sanchez, S. Dietrich and O. G. Schmidt, *Soft Matter*, 2012, **8**, 48–52.
24 L. Soler, V. Magdanz, V. M. Fomin, S. Sanchez and O. G. Schmidt, *ACS Nano*, 2013, **7**, 9611–9620.
25 W. Gao and J. Wang, *ACS Nano*, 2014, **8**, 3170–3180.
26 M. Garcia, J. Orozco, M. Guix, W. Gao, S. Sattayasamitsathit, A. Escarpa, A. Merkoci and J. Wang, *Nanoscale*, 2013, **5**, 1325–1331.
27 S. J. Ebbens and J. R. Howse, *Soft Matter*, 2010, **6**, 726–738.
28 H. Wang and M. Pumera, *Chem. Rev.*, 2015, **115**, 8704–8735.
29 A. I. Campbell, R. Wittkowski, B. ten Hagen, H. Löwen and S. J. Ebbens, 2017, arXiv:1701.06824.
30 F. Kümmel, B. ten Hagen, R. Wittkowski, I. Buttinoni, R. Eichhorn, G. Volpe, H. Löwen and C. Bechinger, *Phys. Rev. Lett.*, 2013, **110**, 198302.
31 B. ten Hagen, F. Kümmel, R. Wittkowski, D. Takagi, H. Löwen and C. Bechinger, *Nat. Commun.*, 2014, **5**, 4829.
32 Y. Li, P. K. Ghosh, F. Marchesoni and B. Li, *Phys. Rev. E: Stat., Nonlinear, Soft Matter Phys.*, 2014, **90**, 062301.
33 M. Mijalkov and G. Volpe, *Soft Matter*, 2013, **9**, 6376–6381.
34 F. Guzmán-Lastra, A. Kaiser and H. Löwen, *Nat. Commun.*, 2016, **7**, 13519.
35 A. Kaiser, K. Popowa and H. Löwen, *Phys. Rev. E: Stat., Nonlinear, Soft Matter Phys.*, 2015, **92**, 012301.
36 R. Soto and R. Golestanian, *Phys. Rev. E: Stat., Nonlinear, Soft Matter Phys.*, 2015, **91**, 052304.
37 R. Soto and R. Golestanian, *Phys. Rev. Lett.*, 2014, **112**, 068301.
38 C. Bechinger, R. Di Leonardo, H. Löwen, C. Reichhardt, G. Volpe and G. Volpe, *Rev. Mod. Phys.*, 2016, **88**, 045006.
39 S. J. Ebbens, *Curr. Opin. Colloid Interface Sci.*, 2016, **21**, 14–23.
40 S. Ni, J. Leemann, I. Buttinoni, L. Isa and H. Wolf, *Sci. Adv.*, 2016, **2**, e1501779.
41 S. Ni, J. Leemann, H. Wolf and L. Isa, *Faraday Discuss.*, 2015, **181**, 225–242.
42 W. D. Ristenpart, I. A. Aksay and D. A. Saville, *J. Fluid Mech.*, 2007, **575**, 83–109.
43 F. Ma, S. Wang, D. T. Wu and N. Wu, *Proc. Natl. Acad. Sci. U. S. A.*, 2015, **112**, 6307–6312.
44 F. Ma, S. Wang, L. Smith and N. Wu, *Adv. Funct. Mater.*, 2012, **22**, 4334–4343.
45 C. Gong, W. Deng, B. Zou, Y. Xing, X. Zhang, X. Zhang and J. Jie, *ACS Appl. Mater. Interfaces*, 2014, **6**, 11018–11024.
46 T. D. Edwards and M. A. Bevan, *Langmuir*, 2014, **30**, 10793–10803.
47 J. Palacci, C. Cottin-Bizonne, C. Ybert and L. Bocquet, *Phys. Rev. Lett.*, 2010, **105**, 088304.
48 B. t. Hagen, S. v. Teeffelen and H. Löwen, *J. Phys.: Condens. Matter*, 2011, **23**, 194119.
49 X. Wang, M. In, C. Blanc, M. Nobili and A. Stocco, *Soft Matter*, 2015, **11**, 7376–7384.
50 S. Ebbens, R. A. L. Jones, A. J. Ryan, R. Golestanian and J. R. Howse, *Phys. Rev. E: Stat., Nonlinear, Soft Matter Phys.*, 2010, **82**, 015304.
51 T. Kraus, L. Malaquin, H. Schmid, W. Riess, N. D. Spencer and H. Wolf, *Nat. Nanotechnol.*, 2007, **2**, 570–576.
52 D. J. Kraft, W. S. Vlug, C. M. van Kats, A. van Blaaderen, A. Imhof and W. K. Kegel, *J. Am. Chem. Soc.*, 2009, **131**, 1182–1186.
53 Y. Wang, Y. Wang, D. R. Breed, V. N. Manoharan, L. Feng, A. D. Hollingsworth, M. Weck and D. J. Pine, *Nature*, 2012, **491**, 51–55.
54 R. W. Perry and V. N. Manoharan, *Soft Matter*, 2016, **12**, 2868–2876.
55 E. Ducrot, M. He, G.-R. Yi and D. J. Pine, *Nat. Mater.*, 2017, **16**, 652–657.